

Quantifying Aleatoric and Epistemic Uncertainty Using Density Estimation in Latent Space

Janis Postels ^{*1} Hermann Blum ^{*1} Cesar Cadena ¹ Roland Siegwart ¹ Luc Van Gool ¹ Federico Tombari ^{2,3}

Abstract

The distribution of a neural network’s latent representations has been successfully used to detect Out-of-Distribution (OOD) data. Since OOD detection denotes a popular benchmark for epistemic uncertainty estimates, this raises the question of a deeper correlation. This work investigates whether the distribution of latent representations indeed contains information about the uncertainty associated with the predictions of a neural network. Prior work identifies epistemic uncertainty with the surprise, thus the negative log-likelihood, of observing a particular latent representation, which we verify empirically. Moreover, we demonstrate that the output-conditional distribution of hidden representations allows quantifying aleatoric uncertainty via the entropy of the predictive distribution. We analyze epistemic and aleatoric uncertainty inferred from the representations of different layers and conclude with the exciting finding that the hidden representations of a deterministic neural network indeed contain information about its uncertainty. We verify our findings on both classification and regression models.

1. Introduction

The recent success of deep neural networks in a variety of applications (Hinton et al., 2012; Redmon et al., 2016; He et al., 2016b; 2017; Chen et al., 2018) has been primarily driven by improvements in predictive performance, while progress on safety-related issues remained relatively slow (Amodei et al., 2016; Bozhinoski et al., 2019; Janai et al., 2017; Sünderhauf et al., 2018). Thereby, quantifying the uncertainty associated with the predictions of a neural network is a central challenge and represents a prerequisite for a broad deployment of deep learning approaches. One

commonly distinguishes between two types of uncertainty (Kiureghian & Ditlevsen, 2009). Uncertainties arising from noise in the data regardless of the choice of model and parameters are called *aleatoric*. Uncertainties originating from the model choice and parameter fitting are referred to as *epistemic*. This differentiation also has practical reasons, since epistemic uncertainty is reducible - e.g. by using more data - while aleatoric uncertainty, as an inherent property of the data, is not.

The predominant research direction for determining a holistic framework for both aleatoric and epistemic uncertainty is Bayesian Deep Learning (BDL) (MacKay, 1992; Hinton & Van Camp, 1993). However, scaling BDL successfully to neural networks of practical size remains an open research question. Although recent research proposed various scalable approaches (Hernández-Lobato & Adams, 2015; Kingma et al., 2015; Gal & Ghahramani, 2016b; Zhang et al., 2017; Teye et al., 2018; Postels et al., 2019), they still fall short of delivering a widely adopted practical solution. Moreover, the quality of the resulting posterior distribution, in particular for scalable approximations, is open for debate (Osband, 2016; Wenzel et al., 2020).

Recent research utilized information extracted from the distribution of a neural network’s latent representations for the task of detecting OOD samples (Ruff et al., 2018; Papernot & McDaniel, 2018; Mandelbaum & Weinshall, 2017; Lee et al., 2018; Alemi et al., 2018; Blum et al., 2019; van Amersfoort et al., 2020). Moreover, density estimates of latent distributions have been implied to yield epistemic uncertainty (Alemi et al., 2018; van Amersfoort et al., 2020). This is a promising avenue, since it allows bypassing scalability issues of BDL by estimating the probability density in the lower-dimensional latent space.

The prospect that the distribution of latent representations holds information about the uncertainty associated with the predictions of a neural network is exciting since it facilitates efficient and scalable uncertainty estimates. It has a particular potential for widespread adoption, because it can be applied post-training independent of the underlying architecture and training methodology. However, a rigorous analysis is necessary. Prior work only evaluated the distribution of hidden representations on separating OOD and training data.

^{*}Equal contribution ¹ETH Zurich ²Google ³Technical University Munich. Correspondence to: Janis Postels <jpostels@ethz.ch>, Hermann Blum <blumh@ethz.ch>.

However, epistemic uncertainty should not only identify far-away OOD samples, but also indicate how well a model can generalize to the given input, thus correlate with model performance in proximity of the training data distribution. Furthermore, it has previously not been investigated whether hidden representations also quantify aleatoric uncertainty. We demonstrate that it is possible to extract the latter by estimating the output-conditional density.

The purpose of this work is to provide a critical analysis and demonstrate that density estimation of the latent distribution in fact gives rise to a holistic framework for the estimation of both epistemic and aleatoric uncertainty. To this end, we examine uncertainty estimates extracted from different architectures and layers of different depth. Aleatoric uncertainty is assessed according to its correlation with the prediction error on the training data distribution. Epistemic uncertainty is evaluated using OOD data - far away from and close to the training data distribution. Moreover, we discuss several practical challenges that arise from uncertainty estimation based on hidden representations (see section 3.3).

Our experiments confirm that the hidden representations indeed contain information about uncertainty. We find further that density estimates of shallow layers give rise to more conservative epistemic uncertainty estimates, while deeper ones behave less conservatively (see section 4.1). While theory suggests that it should be possible to extract aleatoric uncertainty from any layer (see section 3.2), we find that deeper layers make it easier to extract the latter using density estimation.

2. Related Work

2.1. Density Estimation for Out-of-Distribution Detection

Density estimation is an established technique for OOD detection (Pimentel et al., 2014; Schlegl et al., 2017; Chalapathy & Chawla, 2019). While research also developed alternative methods (Pimentel et al., 2014; Liang et al., 2018; Chalapathy & Chawla, 2019), generative models are particularly appealing, since they demonstrate a principled, unsupervised approach to the problem by directly learning the data distribution. To this end, generative models have been trained directly on the data distribution (Schlegl et al., 2017; Li et al., 2018). However, concerns have been voiced regarding their effectiveness (Škvára et al., 2018) and, in particular for explicit generative models, vulnerability to OOD samples (Nalisnick et al., 2019a). Ensembles of generative models (Choi et al., 2018) have been proposed to solve the latter, as well as considering the distribution of log-likelihoods (Nalisnick et al., 2019b; Morningstar et al., 2020).

Since learning high-dimensional densities remains a chal-

lenging task, another line of research focuses on applying traditional machine learning approaches to the latent space of neural networks (Ruff et al., 2018; Papernot & McDaniel, 2018) or directly estimating its density (Mandelbaum & Weinshall, 2017; Lee et al., 2018; Alemi et al., 2018; Blum et al., 2019; van Amersfoort et al., 2020), which is often simpler than for the data itself. In (Mandelbaum & Weinshall, 2017; Lee et al., 2018; van Amersfoort et al., 2020) a Gaussian Mixture Model (GMM) is learned on the representations of a neural network. (Mandelbaum & Weinshall, 2017; van Amersfoort et al., 2020) fix the covariance and (Lee et al., 2018) learns the covariance matrix and applies a subsequent classifier. (Blum et al., 2019) trains a normalizing flow on the latent space. Moreover, (Alemi et al., 2018) utilizes the rate term in the Information Bottleneck (VIB) (Alemi et al., 2016) for OOD detection, which corresponds to the relative entropy between the distribution of the latent representations and a prior distribution.

2.2. Uncertainty Estimation

Uncertainty estimation is related with OOD detection via the fundamental idea that uncertainty should increase outside of the training data distribution. Consequently, uncertainty estimation has been applied to the latter (Hendrycks & Gimpel, 2016; Lee et al., 2017; Li & Gal, 2017; Snoek et al., 2019). We discuss the relation between OOD detection and epistemic uncertainty in detail in section 3.1.

Within uncertainty estimation, Bayesian Neural Networks (Neal, 2012; Neal et al., 2011; Hinton & Van Camp, 1993) constitute the predominant way to quantify uncertainty, since they provide a principled approach for handling both aleatoric and epistemic uncertainty. Due to well known difficulties of applying them to neural networks of practical size, numerous scalable variants have been proposed (Hernández-Lobato & Adams, 2015; Kingma et al., 2015; Gal & Ghahramani, 2016b; Zhang et al., 2017; Teye et al., 2018; Postels et al., 2019). However, current approaches still lack scalability or quality of the predicted uncertainty.

A parallel line of work uses the predictive conditional distribution of neural networks to quantify uncertainty (Bishop, 1994; Hendrycks & Gimpel, 2016; Lee et al., 2017). However, these approaches meet fundamental difficulties outside of the training data distribution. Furthermore, neural networks have been found to be poorly calibrated (Guo et al., 2017), which poses a challenge to all uncertainty estimates.

Recently, it has been suggested that density estimates of a neural network’s latent representations quantify epistemic uncertainty (Mandelbaum & Weinshall, 2017; Alemi et al., 2018; Oh et al., 2018; van Amersfoort et al., 2020). (Mandelbaum & Weinshall, 2017) fits a kernel density to the embeddings. Their score outperforms softmax entropy and Monte-Carlo dropout (Gal & Ghahramani, 2016a) when

imposing an additional regularizing loss on the latent space. (van Amersfoort et al., 2020) replaces the softmax activation with a target-conditional multivariate Gaussian distribution for classification and performs end-to-end training, thus learns a density estimate of the final layer. They refer to the log-likelihood of the density model as epistemic uncertainty and evaluate it on OOD detection. In (Alemi et al., 2018) the authors consider the per-sample rate loss in the VIB objective (Alemi et al., 2016) and the softmax entropy as proxies for uncertainty. They demonstrate that the softmax entropy excels at detecting misclassified in-distribution samples, thus quantifying aleatoric uncertainty, and the rate-loss at OOD detection. Our work essentially reveals that similar conclusions can be drawn for deterministic neural networks that were trained without the VIB objective.

3. Uncertainty Using Density Estimation in Latent Space

3.1. Types of Uncertainty

The goal of uncertainty estimation in machine learning (ML) is to assign a level of confidence to a model’s output. Thus, by definition, the true uncertainty correlates with a model’s performance. While a correct prediction can have high uncertainty, model performance degrades on average where uncertainty increases.

The performance of a model fluctuates within the training data distribution. One reason for this is inherent noise in the training data, which causes irreducible *aleatoric* uncertainty (Kiureghian & Ditlevsen, 2009). Additionally, the performance of a ML model is often dependent on the choice of training data, model, and parameters. Uncertainties and performance drops resulting from these choices are reducible and should be distinguished from their irreducible counterparts. Kiureghian and Ditlevsen (Kiureghian & Ditlevsen, 2009) call these uncertainties ‘*epistemic*’. The same terminology was introduced to the ML community (Senge et al., 2014; Gal, 2016).

As an important failure source, OOD detection is related to uncertainty estimation - in particular epistemic uncertainty. Thus, OOD detection naturally denotes a method for evaluating epistemic uncertainty. However, OOD detection performance alone is not sufficient, since it represents a model agnostic task and epistemic uncertainty should be aligned with a model’s generalization. High epistemic uncertainty is only expected for those OOD samples that lead to degradation of model performance. We investigate this in section 4.1 by applying perturbations of increasing magnitude to the input while tracking estimated uncertainty and model performance. It is worth noting that some works aim at separating *distributional* from *epistemic* uncertainty (Mallin & Gales, 2018; Harang & Rudd, 2018). However, this work follows the definitions from (Kiureghian & Ditlevsen,

2009), where *epistemic* uncertainty encompasses simply all reducible uncertainty.

3.2. Uncertainty of Deterministic Neural Networks

Given a dataset $\mathcal{D} = \{\mathbf{X}, \mathbf{Y}\}$, the goal of a discriminative task is to model the conditional distribution $p(\mathbf{y}|\mathbf{x})$, where $\mathbf{x} \in \mathbf{X}$ and $\mathbf{y} \in \mathbf{Y}$. Let $\hat{\mathbf{y}}$ correspond to the output of a neural network trained to approximate $p(\mathbf{y}|\mathbf{x})$, which induces the conditional distribution $p_\theta(\hat{\mathbf{y}}|\mathbf{x})$. The conditional entropy

$$\begin{aligned} H(\hat{\mathbf{y}}|\mathbf{x}) &= E_{p_\theta(\hat{\mathbf{y}}, \mathbf{x})} [-\log(p_\theta(\hat{\mathbf{y}}|\mathbf{x}))] \\ &= E_{p(\mathbf{x})} \left[- \int d\hat{\mathbf{y}} p_\theta(\hat{\mathbf{y}}|\mathbf{x}) \log(p_\theta(\hat{\mathbf{y}}|\mathbf{x})) \right] \end{aligned} \quad (1)$$

corresponds to the total uncertainty about $\hat{\mathbf{y}}$ given knowledge of \mathbf{x} across the dataset \mathcal{D} . Both quantities under the expectation have been successfully used to quantify aleatoric uncertainty in deterministic neural networks for classification (Hendrycks & Gimpel, 2016; Alemi et al., 2018)¹ and regression (Kendall & Gal, 2017)². The negative log-likelihood $-\log(p_\theta(\hat{\mathbf{y}}|\mathbf{x}))$ is called surprisal or information-content of a particular value $\hat{\mathbf{y}}$ given an input \mathbf{x} . Further, $-\int d\hat{\mathbf{y}} p_\theta(\hat{\mathbf{y}}|\mathbf{x}) \log(p_\theta(\hat{\mathbf{y}}|\mathbf{x}))$ is the expected surprisal for a given input \mathbf{x} .

However, eq. equation 1 only quantifies the uncertainty/surprise about predictions given a specific input \mathbf{x} and not about observing \mathbf{x} in the first place. To account for this, consider the entropy of the joint probability distribution

$$\begin{aligned} H(\hat{\mathbf{y}}, \mathbf{x}) &= H(\mathbf{x}) + H(\hat{\mathbf{y}}|\mathbf{x}) \\ &= E_{p(\mathbf{x})} \left[-\log(p(\mathbf{x})) - \int d\hat{\mathbf{y}} p_\theta(\hat{\mathbf{y}}|\mathbf{x}) \log(p_\theta(\hat{\mathbf{y}}|\mathbf{x})) \right] \end{aligned} \quad (2)$$

In equation 2 the negative log-likelihood $-\log(p(\mathbf{x}))$ quantifies the surprise about observing \mathbf{x} and requires learning the density $p(\mathbf{x})$. Nevertheless, estimating $-\log(p(\mathbf{x}))$ directly would provide an uncertainty estimate independent of the neural network used to parameterize $p_\theta(\hat{\mathbf{y}}|\mathbf{x})$. Thus, it does not take the neural network’s generalization into account and can be considered a model-agnostic distributional uncertainty. Moreover, this distributional uncertainty incorporates the entire information in the distribution of \mathbf{X}

¹In fact, (Hendrycks & Gimpel, 2016) uses the maximum softmax probability. However, this does not change the ordering of the uncertainty values, since the logarithm is a strictly monotonic function. Thus, the log-probability produces equivalent results.

²The authors parameterize the output with a unimodal Gaussian and use its variance as aleatoric uncertainty. In this case the entropy is proportional to the logarithm of the variance.

- especially also information irrelevant for the discriminative task. An additional practical problem arises when \mathbf{X} is high-dimensional, since learning high-dimensional densities denotes a challenging research question.

Therefore, let a neural network be comprised of L layers with $L - 1$ latent representations $(\mathbf{z}_0, \dots, \mathbf{z}_{L-2})$ and let the joint distribution factorize according to $p_\theta(\mathbf{x}, \hat{\mathbf{y}}, \mathbf{z}_0, \dots, \mathbf{z}_{L-2}) = p_\theta(\hat{\mathbf{y}}|\mathbf{z}_{L-2})p(\mathbf{z}_{L-2}|\mathbf{z}_{L-3}) \dots p_\theta(\mathbf{z}_0|\mathbf{x})p(\mathbf{x})$. Exploiting the deterministic nature of the neural network and the data processing inequality allows us to make the following statements:

$$H(\hat{\mathbf{y}}|\mathbf{z}_i) = H(\hat{\mathbf{y}}|\mathbf{x}) \quad \forall i \in [0, \dots, L-2]$$

$$H(\mathbf{x}) \geq H(\mathbf{z}_0) \geq \dots \geq H(\mathbf{z}_{L-2})$$

See appendix A.1.1 for a detailed derivation. These inequalities relate the distribution of the latent representations to the uncertainties in equation 2. Since the entropy denotes the expected surprise, uncertainty estimates based on deeper layers are less conservative. On the other side, since the distribution of the latent space at a particular layer is a functional of all the previous layers, we expect these uncertainty estimates to incorporate some degree of model dependence. We verify these claims empirically in section 4.1 by detecting OOD samples using density estimate of different layers.

We also investigate whether information about aleatoric uncertainty can be extracted from the latent distribution. To also access the latter in such cases, we learn the joint density $p(\mathbf{z}_i, \hat{\mathbf{y}})$ at layer i . This can be achieved by separately estimating the output-conditional distribution $p(\mathbf{z}_i|\hat{\mathbf{y}})$ and $p(\hat{\mathbf{y}})$. Using Bayes formula and marginalization over $\hat{\mathbf{y}}$, we can compute both values under the expectations in Eq. equation 1. In section 4.1 we find empirically that deeper layers enable better aleatoric uncertainty estimates. We hypothesize that this results from the neural network filtering out task-irrelevant information, which makes it easier to estimate the output-conditional density.

To summarize, given a novel input \mathbf{x}^* with corresponding latent vector \mathbf{z}_i^* , we identify the epistemic uncertainty with the surprise of observing that latent representation $-\log p(\mathbf{z}_i^*)$ and the aleatoric uncertainty with the expected surprisal of $\hat{\mathbf{y}} \sim p(\hat{\mathbf{y}}|\mathbf{z}_i^*)$ which we subsequently denote with $h(\hat{\mathbf{y}}|\mathbf{z}_i^*)$ for convenience:

$$-\log p(\mathbf{z}^*) = -\log \left(\int d\hat{\mathbf{y}} p(\mathbf{z}^*|\hat{\mathbf{y}})p(\hat{\mathbf{y}}) \right) \quad (3)$$

$$h(\hat{\mathbf{y}}|\mathbf{z}_i^*) = - \int d\hat{\mathbf{y}} p_\theta(\hat{\mathbf{y}}|\mathbf{z}_i^*) \log (p_\theta(\hat{\mathbf{y}}|\mathbf{z}_i^*)) \quad (4)$$

In the rest of this work we may choose to use $\log p(\mathbf{z}_i^*)$ instead of $-\log p(\mathbf{z}_i^*)$, which can be interpreted as certainty,

without reducing the validity of our statements about uncertainty quality.

3.3. Pitfalls

In some cases, especially when considering large neural networks or shallow layers, the dimensionality of the hidden representations remains extremely high. This renders estimating their density impractical. We note that prior work using high-dimensional hidden representations has also faced the curse of dimensionality. For example (Lee et al., 2018) reduced the dimensionality of hidden representations by performing Principal Component Analysis (PCA) on the training data distribution and, subsequently, reusing the transformation at inference time. Moreover, (Papernot & McDaniel, 2018) uses locality sensitive hashing in combination with random projections for nearest neighbour search. In this work we follow (Lee et al., 2018) applying PCA and find that it yields satisfying results in practice. However, we note that PCA as well as random projections are not optimal solutions in the case of convolutional neural networks which hidden representations entail translational invariances. These are ignored by dense projection matrices used in PCA and random projections.

Another practical challenge when using the distribution of hidden representations for uncertainty quantification is connected to the strengths of discriminative neural networks. During training the latter learns to ignore task-irrelevant features of the data. However, this can lead to activations of OOD data becoming indistinguishable from activations of the training data. Some prior work has partially noted this problem (Mandelbaum & Weinshall, 2017; van Amersfoort et al., 2020). Nevertheless, proposed solutions to this problem commonly lead to difficult hyperparameter optimization which trades off predictive performance with OOD detection. (Mandelbaum & Weinshall, 2017) introduces an additional distance regularization loss between hidden representations. Moreover, (Mandelbaum & Weinshall, 2017), referring to the problem as feature collapse, introduces an expensive gradient penalty that requires optimizing the gradients regarding the inputs of the neural network. Further, note that, although (Alemi et al., 2018) does not mention this problem explicitly, training with the VIB framework regularizes the distribution of hidden representations according to a prior distribution. In this work, we do not intervene with the training procedure and accept the possibility of reduced uncertainty quality, since our goal is to investigate the performance under unaltered training procedure. This lets us draw conclusions about how effective this widely - and especially post-training - applicable approach can be.

3.4. Implementation

This work studies density based uncertainty estimates independently of the underlying network and training. In order to then estimate epistemic (equation 3) and aleatoric uncertainty (equation 4), we extract the latent representations of a particular layer i and learn the output-conditional density $p(\mathbf{z}_i|\hat{\mathbf{y}})$ and the distribution of the neural network's outputs $p(\hat{\mathbf{y}})$ on the training data.

$p(\mathbf{z}_i|\hat{\mathbf{y}})$ can be learned using an explicit generative model. In our experiments on image classification (see section 4.1 and A.4) we use one GMM with $k \in \mathbb{N}_{\setminus\{0\}}$ components for each class. In case of regression (see section 4.2 and A.5), we use conditional normalizing flows (CNFs). While there are several ways to implement CNFs, we found the conditioning scheme used in (Ardizzone et al., 2019) to yield good results. We refer the reader to the supplementary material for details.

Estimating $p(\hat{\mathbf{y}})$ for a classification task simply involves counting the predicted labels on the training data distribution. For a regression task, however, it is necessary to estimate the density of the predictions in the output space. This is relatively simple, since the output space is low dimensional for most common discriminative tasks. In this work we found it sufficient to approximate it with a univariate parametric distribution - a uniform distribution in section 4.2 and a betaprime distribution for the predicted depth in section A.5.

We then obtain the epistemic uncertainty in eq. equation 3 by marginalizing $\hat{\mathbf{y}}$. To solve the integral, we use summation (classification) or numerical integration (regression). We found the latter to be sufficient for the one dimensional output spaces in our regression experiments (see section 4.2 and A.5). Subsequently, we calculate the aleatoric uncertainty in eq. equation 4 by plugging $p(\mathbf{z}_i)$, $p(\mathbf{z}_i|\hat{\mathbf{y}})$ and $p(\hat{\mathbf{y}})$ into Bayes formula.

4. Experiments

While there exists no ground truth for uncertainty, we follow the approach of other works (Gal & Ghahramani, 2016a; Lakshminarayanan et al., 2017; Malinin & Gales, 2018) and examine epistemic uncertainty over input transformations and distributional shifts and aleatoric uncertainty via the correlation with the network's predictive performance on in-distribution data. Section 4.1 investigates the behaviour of uncertainties extracted from the output-conditional density depending on the depth of the representations on image classification. Section 4.2 validates this approach for the task of regression on a toy dataset. Furthermore, we refer to the supplementary material for experiments using very large neural networks for semantic segmentation and depth regression.

The goal of this section is twofold. Section 4.1.1 analyses the estimated epistemic uncertainty from latent representations of varying depth, when leaving the training data distribution in small discrete steps using additive Gaussian noise and rotations. We expect epistemic uncertainty to correlate with model generalization, which is the observed behaviour of established methods such as MC Dropout (Gal & Ghahramani, 2016b) and Deep Ensembles (Lakshminarayanan et al., 2017). We chose to compare with these methods due to their popularity and scalability. Furthermore, we investigate the calibration of aleatoric uncertainty on the training data distribution. Then, section 4.1.2 examines the OOD performance of the epistemic uncertainty.

For both experiments, we train a multilayer perceptron (FC-Net) consisting of fully-connected layers and ReLU activations on MNIST (LeCun et al., 1998) and FashionMNIST (Xiao et al., 2017) and ResNet 18 (He et al., 2016a) (resnet) on CIFAR10 (Krizhevsky et al., 2009) and SVHN (Netzer et al., 2011). We use the same architectures in the basis for MC Dropout and Deep Ensembles. After training the above networks, we extract intermediate activations directly after affine layers of varying depth and estimate the output-conditional density of these latent representations. Since the hidden representations of resnet - especially the ones of shallow layers - are very high dimensional, we reduce their dimensionality to 512 using PCA (see section 3.3). We visualize the quality of the reulsting fit for different layers in the supplementary material, where we also report all experimental details.

4.1. Image Classification

4.1.1. QUALITY OF UNCERTAINTY DEPENDING ON DEPTH

We estimate the density of the hidden representations on the training data of FCNet trained on MNIST and of resnet trained on SVHN using a GMM. Each training and subsequent density estimation is conducted five times independently yielding mean and standard deviation of our results. We quantify epistemic and aleatoric uncertainty according to eq. 3 and eq. 4.

First, we evaluate the behaviour of the epistemic uncertainty estimate when leaving the training data distribution in small discrete steps. Therefore, we compute the AUROC between the unperturbed testset and each perturbation magnitude. The AUROC measures how well a binary classifier identifies the perturbed test samples based on the estimated epistemic uncertainty. On MNIST we rotate test samples from 0° to 180° in 20° steps and on SVHN we add independent Gaussian noise to the pixel values of input images, while increasing the standard deviation from 0 to 80 with step size 10. Fig. 1 shows the results ((a) MNIST (b) SVHN). The left plots visualize the accuracy of the corresponding

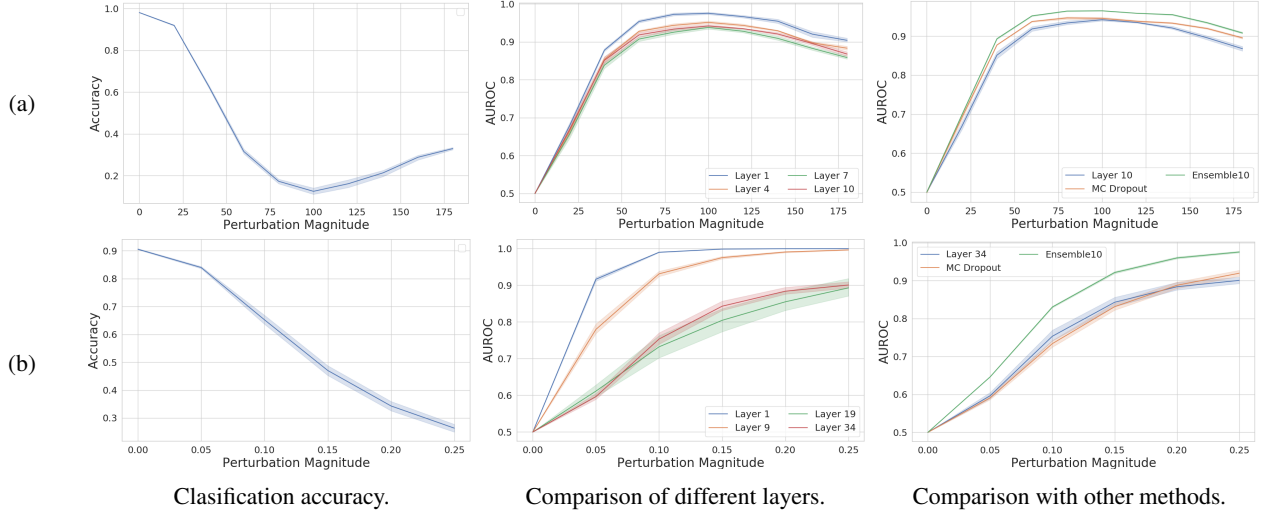


Figure 1: Analysis of the quality of estimated epistemic uncertainty over different layers for FCNet on MNIST **(a)**, and resnet on SVHN **(b)**. We plot the accuracy of the classification network (**left**) and the Area Under the ROC curve (obtained using epistemic uncertainty as threshold) against the perturbation magnitude on the test data (**center** and **right**). We compare epistemic uncertainty obtained from hidden representations of varying depth (**center**) and other methods (**right**). We observe that 1) density estimates based on deeper layers behave similar as other established - but computationally more expensive - methods (i.e. MC Dropout and Deep Ensembles) and 2) that density estimates based on shallow layers yield more conservative estimates.

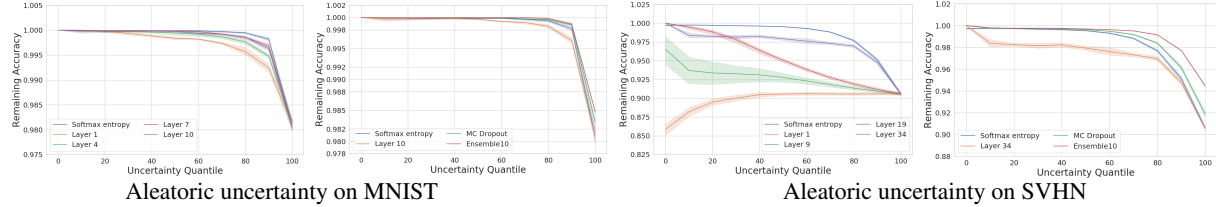


Figure 2: Analysis of the calibration of aleatoric uncertainty on MNIST (**left**) and SVHN (**right**). We plot the remaining accuracy when selecting test samples using incrementally increased aleatoric uncertainty threshold. We observe that aleatoric uncertainty obtained from deeper layers tends to behave similar as other approaches (softmax entropy, Deep Ensembles, MC Dropout).

classifier. The center of Fig. 1 compares epistemic uncertainty estimates obtained from layers of varying depth and the right side compares epistemic uncertainty obtained from hidden representations with common scalable approaches. Epistemic uncertainty of MC Dropout and Deep Ensembles is computed as the mutual information between the predictions and the weights (Gal et al., 2017).

We observe that the epistemic uncertainty obtained from density estimates from shallow layers behave more conservative in the sense that they are quicker to label perturbed data as OOD. On the other side, epistemic uncertainty from deeper layers behaves less conservative and similar as MC Dropout and Deep Ensembles, while only requiring training one model and performing one forward pass.

Fig. 2 analyzes the quality of the estimated aleatoric uncertainty using calibration curves. These show the accuracy of the neural network depending on the uncertainty. Therefore, we use a threshold sliding through increasing percentiles of the aleatoric uncertainty and plot the corresponding remaining accuracy. Ideally this yields a strictly monotonically decreasing curve. We compare aleatoric uncertainty obtained from various layers, MC Dropout, Deep Ensembles and the softmax entropy. Aleatoric uncertainty of MC Dropout and Deep Ensembles is computed as the difference between the total uncertainty and the mutual information between the predictions and the weights (Gal et al., 2017).

Our experiments show that aleatoric uncertainty obtained from density estimates of deeper layers demonstrate similar calibration curves as established approaches. However,

Dataset / OOD Dataset	Layer 1	Layer 4	Layer 7	Layer 10	Ensemble
Trained on MNIST					
FashionMNIST	0.975 ± 0.001	0.922 ± 0.013	0.855 ± 0.032	0.811 ± 0.035	0.896 ± 0.018
OMNIGLOT	0.972 ± 0.002	0.937 ± 0.006	0.892 ± 0.006	0.893 ± 0.011	0.979 ± 0.001
Gaussian noise	1.000 ± 0.000	0.972 ± 0.005	0.903 ± 0.005	0.841 ± 0.010	0.785 ± 0.005
Rotated (90°)	0.978 ± 0.001	0.976 ± 0.004	0.950 ± 0.005	0.935 ± 0.006	0.965 ± 0.002
HFlip	0.902 ± 0.002	0.907 ± 0.005	0.883 ± 0.007	0.864 ± 0.007	0.905 ± 0.001
VFlip	0.887 ± 0.001	0.868 ± 0.002	0.851 ± 0.004	0.830 ± 0.012	0.881 ± 0.002
Trained on FashionMNIST					
MNIST	0.985 ± 0.001	0.991 ± 0.003	0.975 ± 0.004	0.978 ± 0.005	0.962 ± 0.004
OMNIGLOT	0.971 ± 0.001	0.987 ± 0.002	0.960 ± 0.012	0.967 ± 0.008	0.960 ± 0.003
Gaussian noise	1.000 ± 0.000	0.985 ± 0.002	0.971 ± 0.006	0.930 ± 0.013	0.840 ± 0.004
Rotated (90°)	0.884 ± 0.002	0.780 ± 0.045	0.804 ± 0.030	0.835 ± 0.013	0.670 ± 0.013
HFlip	0.719 ± 0.003	0.696 ± 0.007	0.701 ± 0.010	0.693 ± 0.008	0.657 ± 0.010
VFlip	0.898 ± 0.006	0.891 ± 0.014	0.891 ± 0.006	0.901 ± 0.013	0.845 ± 0.014

Table 1: OOD performance in terms of AUROC on various datasets when estimating epistemic uncertainty using the hidden activations of a multilayer perceptron on MNIST and FashionMNIST. We evaluate AUROC using the epistemic uncertainty computed from the distribution of the output of several affine layers (1, 4, 7, 10). For comparison, we further report the performance of an ensemble of 10 neural networks of identical architecture. We observe that uncertainty estimates based on shallow layers demonstrate strong OOD performance.

aleatoric uncertainty based on shallow layers can perform poorly (see right side of 2), as can be seen in the results for resnet on SVHN. As discussed in section 3.3, we argue that this poor performance results from estimating the density of very high-dimensional hidden representations.

4.1.2. OOD PERFORMANCE OF EPISTEMIC UNCERTAINTY

This experiment evaluates the OOD detection performance of epistemic uncertainty. We evaluate FCNet trained on MNIST/FashionMNIST (table 1) and resnet trained on CIFAR10/SVHN (table 2). Each result is comprised of mean and standard deviation obtained from five independent trainings. We measure OOD detection performance in terms of AUROC when evaluating on OOD data. When training on MNIST/FashionMNIST we evaluate on FashionMNIST/MNIST, OMNIGLOT (Lake et al., 2015), test data perturbed with additive Gaussian noise, rotated test data (90°) and horizontally and vertically flipped test data. When training on CIFAR10/SVHN we evaluate on SVHN/CIFAR10, STL10 (Coates et al., 2011), test data perturbed with additive Gaussian noise, rotated test data (90°) and horizontally and vertically flipped test data. We compare the OOD performance with the one of epistemic uncertainty obtained from Deep Ensembles.

We generally observe a strong performance of epistemic uncertainty obtained from shallow layers which coincides with the results of section 4.1.1, where we found that shallow layers yield more conservative estimates. However, we find that, when using a convolutional architecture (resnet), epistemic uncertainty obtained from shallow layers fails to

detect OOD data generated by globally transforming the test data. We argue that this is expected behaviour since the hidden representations of shallow layers in convolutional networks denote low-level features that are likely to not represent such global transformations. Finally, we note the poor performance of shallow layers when training on CIFAR10 and evaluating on SVHN. These results suggest that recently found difficulties of explicit generative models on the task of OOD detection also apply to shallow layers. However, epistemic uncertainty from deeper layers does not suffer from this problem.

4.2. Regression

As a simple regression experiment, we train regressors on data sampled from $f(x) = \frac{1}{2} (\sin(4\pi x - \frac{\pi}{2}) + x)$ for $x \in [-1, 1]$ ³. The training data and methods are illustrated in figure 3. We evaluate the estimate of epistemic uncertainty in the gap of the training data. Experimental details can be found in the supplementary material. For inference, we perform numerical integration to evaluate the likelihood of the latent vectors.

Figure 3 shows a comparison of the latent density approach (a) to a Bayesian Deep Learning method (Lakshminarayanan et al., 2017) (b) and a Gaussian process (c). The estimated uncertainty for each method is shown in violet elevation surfaces. All methods show growing uncertainty with further distance to the training data, indicating that latent densities also carry uncertainty information about

³The function was designed to be naturally normalised to $[-1, 1] \rightarrow [-1, 1]$

Dataset / OOD Dataset	Layer 1	Layer 9	Layer 19	Layer 34	Ensemble
Trained on SVHN					
CIFAR10	0.991 ± 0.001	0.974 ± 0.004	0.934 ± 0.008	0.907 ± 0.003	0.976 ± 0.002
STL10	0.999 ± 0.000	0.991 ± 0.002	0.951 ± 0.009	0.912 ± 0.003	0.982 ± 0.002
Gaussian noise	1.000 ± 0.000	1.000 ± 0.000	0.986 ± 0.011	0.903 ± 0.016	0.992 ± 0.002
Rotated (90°)	0.615 ± 0.001	0.646 ± 0.010	0.689 ± 0.024	0.918 ± 0.002	0.957 ± 0.002
HFlip	0.500 ± 0.000	0.503 ± 0.005	0.495 ± 0.010	0.500 ± 0.002	0.501 ± 0.002
VFlip	0.506 ± 0.000	0.520 ± 0.004	0.551 ± 0.010	0.708 ± 0.006	0.736 ± 0.001
Trained on CIFAR10					
SVHN	0.042 ± 0.001	0.029 ± 0.004	0.091 ± 0.016	0.736 ± 0.055	0.723 ± 0.048
STL10	0.790 ± 0.010	0.871 ± 0.019	0.821 ± 0.038	0.651 ± 0.008	0.806 ± 0.004
Gaussian noise	1.000 ± 0.000	1.000 ± 0.000	1.000 ± 0.000	0.681 ± 0.057	0.999 ± 0.002
Rotated (90°)	0.553 ± 0.003	0.517 ± 0.020	0.543 ± 0.005	0.757 ± 0.001	0.824 ± 0.003
HFlip	0.500 ± 0.000	0.500 ± 0.000	0.499 ± 0.001	0.500 ± 0.002	0.501 ± 0.001
VFlip	0.519 ± 0.003	0.513 ± 0.006	0.537 ± 0.006	0.714 ± 0.001	0.789 ± 0.004

Table 2: OOD performance in terms of AUROC on various datasets when estimating epistemic uncertainty using the hidden activations of a resnet 18 on SVHN and CIFAR10. We evaluate AUROC using the epistemic uncertainty computed from the distribution of the output of several affine layers (1, 9, 19, 134). For comparison, we further report the performance of a deep ensemble of 10 neural networks of identical architecture. We observe that uncertainty estimates based on shallow layers demonstrate strong OOD performance.

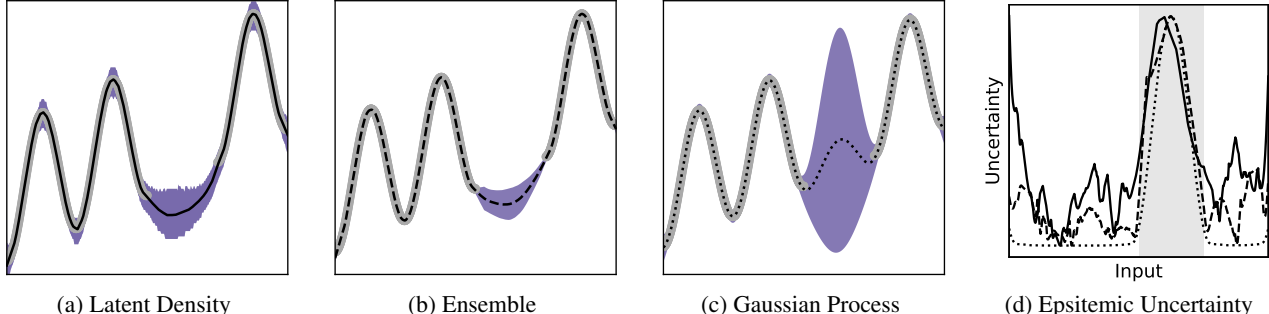


Figure 3: Simple regression task. The models are trained only on the data outlined in gray. (a-c): Model prediction is given in black and the high-confidence area in blue. In (d), we compare the estimated epistemic uncertainty of latent density (solid), bayesian ensemble (dashed) and a GP (dotted). The gray background indicates the gap in the training data.

epistemic uncertainty in regression networks. For a better evaluation, we compare $-\log p(\mathbf{z}_i^*)$ against other epistemic uncertainty methods in figure 3d. We observe that all methods follow the expected behaviour of high uncertainty in the gray data gap and low uncertainty in the region of the training data, while this uncertainty is slightly increasing towards the boundaries of the training distribution for the ensemble and the latent density.

5. Discussion & Conclusion

This work introduced a holistic framework for uncertainty estimation based on the density of latent representations and verified its effectiveness empirically. We found that latent representations of shallow layers yield more conservative uncertainty estimates, while deeper layers tend to be less conservative (see section 4.1). Moreover, section 4.1.1 demonstrates that epistemic uncertainty obtained

from deeper layers behaves similarly as MC Dropout and Deep Ensembles when applying perturbations of increasing magnitude to the test data. We therefore showed that latent densities do not merely model distance to training data, but indicate a model's ability to generalize to the given data. This has promising practical implications since evaluating the latent density is computationally much cheaper and can be applied to any neural network post-training. The latter is particularly important, since it implies hidden information in neural networks that allows quantifying trust in their predictions and consequently enables rapid application of our framework to already trained models. Furthermore, we also demonstrated that the proposed framework can be applied to regression (see section 4.2).

Section 4.1.2 investigated the OOD performance of epistemic uncertainty and concludes that epistemic uncertainty from shallow layers has superior performance, which is in line with the results in section 4.1.1. They even outperform

Deep Ensembles for various OOD datasets, while adding negligible computational overhead and leaving the training procedure unchanged. However, we also find that certain global perturbations of the data distribution are better detected using the density of deeper layers. This suggests that the task of OOD detection can benefit from aggregating uncertainty information from several layers. We leave this exploration for future work. In fact, (Lee et al., 2018) utilizes density estimates from several layers. However, thus far they require logistic regression trained on OOD data for merging the results from several layers.

Moreover, section 4.1.2 shed light onto a recently observed phenomenon in related work, namely that density models trained on CIFAR10 yield higher log-likelihoods on SVHN than on CIFAR10 (Nalisnick et al., 2019a; Choi et al., 2018). Our experiments suggest that similar conclusions hold for the distribution of representations of shallow layers. However, the distribution of deeper layers appears to be more robust to this phenomenon.

While this work proposes a promising framework applicable to any neural network, it also opens up avenues for future research. We intentionally did not alter the training procedure in order to evaluate what quality of uncertainty one can expect for neural networks using default training procedures. We intend to conduct future research towards techniques that perform minimal invasive changes at training time such that latent representations yield improved uncertainty estimates.

References

Alemi, A. A., Fischer, I., Dillon, J. V., and Murphy, K. Deep variational information bottleneck. *Proceedings of the International Conference on Learning Representations (ICLR) 2017*, 2016.

Alemi, A. A., Fischer, I., and Dillon, J. V. Uncertainty in the variational information bottleneck. *arXiv preprint arXiv:1807.00906*, 2018.

Amodei, D., Olah, C., Steinhardt, J., Christiano, P., Schulman, J., and Mané, D. Concrete problems in ai safety. *arXiv preprint arXiv:1606.06565*, 2016.

Ardizzone, L., Lüth, C., Kruse, J., Rother, C., and Köthe, U. Guided image generation with conditional invertible neural networks. *arXiv preprint arXiv:1907.02392*, 2019.

Bishop, C. M. Mixture density networks. *Aston University*, 1994.

Blum, H., Sarlin, P.-E., Nieto, J., Siegwart, R., and Cadena, C. The fishyscapes benchmark: Measuring blind spots in semantic segmentation. *arXiv preprint arXiv:1904.03215*, 2019.

Bozhinoski, D., Di Ruscio, D., Malavolta, I., Pelliccione, P., and Crnkovic, I. Safety for mobile robotic systems: A systematic mapping study from a software engineering perspective. *Journal of Systems and Software*, 151:150–179, 2019.

Chalapathy, R. and Chawla, S. Deep learning for anomaly detection: A survey. *arXiv preprint arXiv:1901.03407*, 2019.

Chen, L.-C., Zhu, Y., Papandreou, G., Schroff, F., and Adam, H. Encoder-decoder with atrous separable convolution for semantic image segmentation. In *Proceedings of the European conference on computer vision (ECCV)*, pp. 801–818, 2018.

Choi, H., Jang, E., and Alemi, A. A. Waic, but why? generative ensembles for robust anomaly detection. *arXiv preprint arXiv:1810.01392*, 2018.

Coates, A., Ng, A., and Lee, H. An analysis of single-layer networks in unsupervised feature learning. In *Proceedings of the fourteenth international conference on artificial intelligence and statistics*, pp. 215–223, 2011.

Cordts, M., Omran, M., Ramos, S., Rehfeld, T., Enzweiler, M., Benenson, R., Franke, U., Roth, S., and Schiele, B. The cityscapes dataset for semantic urban scene understanding. In *2016 IEEE Conference on Computer Vision and Pattern Recognition (CVPR)*, pp. 3213–3223, June 2016a. doi: 10.1109/CVPR.2016.350.

Cordts, M., Omran, M., Ramos, S., Rehfeld, T., Enzweiler, M., Benenson, R., Franke, U., Roth, S., and Schiele, B. The cityscapes dataset for semantic urban scene understanding. In *Proc. of the IEEE Conference on Computer Vision and Pattern Recognition (CVPR)*, 2016b.

Dinh, L., Krueger, D., and Bengio, Y. Nice: Non-linear independent components estimation. *arXiv preprint arXiv:1410.8516*, 2014.

Dinh, L., Sohl-Dickstein, J., and Bengio, S. Density estimation using real nvp. *International Conference on Learning Representations*, 2017.

Gal, Y. Uncertainty in deep learning. *University of Cambridge*, 1:3, 2016.

Gal, Y. and Ghahramani, Z. Dropout as a bayesian approximation: Representing model uncertainty in deep learning. In Balcan, M. F. and Weinberger, K. Q. (eds.), *Proceedings of The 33rd International Conference on Machine Learning*, volume 48 of *Proceedings of Machine Learning Research*, pp. 1050–1059, New York, New York, USA, 2016a. PMLR.

Gal, Y. and Ghahramani, Z. Dropout as a bayesian approximation: Representing model uncertainty in deep learning. In *international conference on machine learning*, pp. 1050–1059, 2016b.

Gal, Y., Islam, R., and Ghahramani, Z. Deep bayesian active learning with image data. In *Proceedings of the 34th International Conference on Machine Learning-Volume 70*, pp. 1183–1192. JMLR. org, 2017.

Geiger, A., Lenz, P., and Urtasun, R. Are we ready for autonomous driving? the kitti vision benchmark suite. In *Conference on Computer Vision and Pattern Recognition (CVPR)*, 2012.

Godard, C., Mac Aodha, O., and Brostow, G. J. Unsupervised monocular depth estimation with left-right consistency. In *Proceedings of the IEEE Conference on Computer Vision and Pattern Recognition*, pp. 270–279, 2017.

Guo, C., Pleiss, G., Sun, Y., and Weinberger, K. Q. On calibration of modern neural networks. In *Proceedings of the 34th International Conference on Machine Learning-Volume 70*, pp. 1321–1330. JMLR. org, 2017.

Harang, R. and Rudd, E. M. Towards principled uncertainty estimation for deep neural networks. *arXiv preprint arXiv:1810.12278*, 2018.

He, K., Zhang, X., Ren, S., and Sun, J. Deep residual learning for image recognition. In *Proceedings of the IEEE conference on computer vision and pattern recognition*, pp. 770–778, 2016a.

He, K., Zhang, X., Ren, S., and Sun, J. Deep residual learning for image recognition. In *Proceedings of the IEEE conference on computer vision and pattern recognition*, pp. 770–778, 2016b.

He, K., Gkioxari, G., Dollar, P., and Girshick, R. Mask R-CNN. In *2017 IEEE International Conference on Computer Vision (ICCV)*, pp. 2980–2988. IEEE, October 2017. ISBN 9781538610329. doi: 10.1109/ICCV.2017.322.

Hendrycks, D. and Gimpel, K. A baseline for detecting misclassified and out-of-distribution examples in neural networks. *arXiv preprint arXiv:1610.02136*, 2016.

Hernández-Lobato, J. M. and Adams, R. Probabilistic back-propagation for scalable learning of bayesian neural networks. In *International Conference on Machine Learning*, pp. 1861–1869, 2015.

Hinton, G., Deng, L., Yu, D., Dahl, G. E., Mohamed, A.-r., Jaitly, N., Senior, A., Vanhoucke, V., Nguyen, P., Sainath, T. N., et al. Deep neural networks for acoustic modeling in speech recognition: The shared views of four research groups. *IEEE Signal processing magazine*, 29(6):82–97, 2012.

Hinton, G. E. and Van Camp, D. Keeping the neural networks simple by minimizing the description length of the weights. In *Proceedings of the sixth annual conference on Computational learning theory*, pp. 5–13, 1993.

Janai, J., Güney, F., Behl, A., and Geiger, A. Computer vision for autonomous vehicles: Problems, datasets and state-of-the-art. *arXiv preprint arXiv:1704.05519*, 2017.

Kendall, A. and Gal, Y. What uncertainties do we need in bayesian deep learning for computer vision? In *Advances in neural information processing systems*, pp. 5574–5584, 2017.

Kingma, D. P. and Ba, J. Adam: A method for stochastic optimization. *arXiv preprint arXiv:1412.6980*, 2014.

Kingma, D. P., Salimans, T., and Welling, M. Variational dropout and the local reparameterization trick. In *Advances in neural information processing systems*, pp. 2575–2583, 2015.

Kiureghian, A. D. and Ditlevsen, O. Aleatory or epistemic? does it matter? *Structural Safety*, 31(2):105–112, March 2009. ISSN 0167-4730. doi: 10.1016/j.strusafe.2008.06.020.

Krizhevsky, A., Hinton, G., et al. Learning multiple layers of features from tiny images. *Citeseer*, 2009.

Lake, B. M., Salakhutdinov, R., and Tenenbaum, J. B. Human-level concept learning through probabilistic program induction. *Science*, 350(6266):1332–1338, 2015.

Lakshminarayanan, B., Pritzel, A., and Blundell, C. Simple and scalable predictive uncertainty estimation using deep ensembles. In *Advances in neural information processing systems*, pp. 6402–6413, 2017.

LeCun, Y., Bottou, L., Bengio, Y., and Haffner, P. Gradient-based learning applied to document recognition. *Proceedings of the IEEE*, 86(11):2278–2324, 1998.

Lee, K., Lee, H., Lee, K., and Shin, J. Training confidence-calibrated classifiers for detecting out-of-distribution samples. *arXiv preprint arXiv:1711.09325*, 2017.

Lee, K., Lee, K., Lee, H., and Shin, J. A simple unified framework for detecting out-of-distribution samples and adversarial attacks. In *Advances in Neural Information Processing Systems*, pp. 7167–7177, 2018.

Li, D., Chen, D., Goh, J., and Ng, S.-K. Anomaly detection with generative adversarial networks for multivariate time series. *arXiv preprint arXiv:1809.04758*, 2018.

Li, Y. and Gal, Y. Dropout inference in bayesian neural networks with alpha-divergences. In *Proceedings of the 34th International Conference on Machine Learning-Volume 70*, pp. 2052–2061. JMLR. org, 2017.

Liang, S., Li, Y., and Srikant, R. Enhancing the reliability of out-of-distribution image detection in neural networks. *International Conference on Learning Representations*, 2018.

MacKay, D. J. A practical bayesian framework for backpropagation networks. *Neural computation*, 4(3):448–472, 1992.

Malinin, A. and Gales, M. Predictive uncertainty estimation via prior networks. In *Advances in Neural Information Processing Systems*, pp. 7047–7058, 2018.

Mandelbaum, A. and Weinshall, D. Distance-based confidence score for neural network classifiers. *arXiv preprint arXiv:1709.09844*, 2017.

Morningstar, W. R., Ham, C., Gallagher, A. G., Lakshminarayanan, B., Alemi, A. A., and Dillon, J. V. Density of states estimation for out-of-distribution detection. *arXiv preprint arXiv:2006.09273*, 2020.

Nalisnick, E., Matsukawa, A., Teh, Y. W., Gorur, D., and Lakshminarayanan, B. Do deep generative models know what they don’t know? *International Conference on Learning Representations*, 2019a.

Nalisnick, E., Matsukawa, A., Teh, Y. W., and Lakshminarayanan, B. Detecting out-of-distribution inputs to deep generative models using typicality. *arXiv preprint arXiv:1906.02994*, 2019b.

Neal, R. M. *Bayesian learning for neural networks*, volume 118. Springer Science & Business Media, 2012.

Neal, R. M. et al. Mcmc using hamiltonian dynamics. *Handbook of markov chain monte carlo*, 2(11):2, 2011.

Netzer, Y., Wang, T., Coates, A., Bissacco, A., Wu, B., and Ng, A. Y. Reading digits in natural images with unsupervised feature learning. *Citeseer*, 2011.

Oh, S. J., Murphy, K., Pan, J., Roth, J., Schroff, F., and Gallagher, A. Modeling uncertainty with hedged instance embedding. *arXiv preprint arXiv:1810.00319*, 2018.

Osband, I. Risk versus uncertainty in deep learning: Bayes, bootstrap and the dangers of dropout. In *NIPS Workshop on Bayesian Deep Learning*, volume 192, 2016.

Papernot, N. and McDaniel, P. Deep k-nearest neighbors: Towards confident, interpretable and robust deep learning. *arXiv preprint arXiv:1803.04765*, 2018.

Pimentel, M. A., Clifton, D. A., Clifton, L., and Tarassenko, L. A review of novelty detection. *Signal Processing*, 99: 215–249, 2014.

Pinggera, P., Ramos, S., Gehrig, S., Franke, U., Rother, C., and Mester, R. Lost and found: detecting small road hazards for self-driving vehicles. In *2016 IEEE/RSJ International Conference on Intelligent Robots and Systems (IROS)*, 2016.

Postels, J., Ferroni, F., Coskun, H., Navab, N., and Tombari, F. Sampling-free epistemic uncertainty estimation using approximated variance propagation. In *Proceedings of the IEEE International Conference on Computer Vision*, pp. 2931–2940, 2019.

Redmon, J., Divvala, S., Girshick, R., and Farhadi, A. You only look once: Unified, Real-Time object detection. In *2016 IEEE Conference on Computer Vision and Pattern Recognition (CVPR)*, pp. 779–788. IEEE, June 2016. ISBN 9781467388511. doi: 10.1109/CVPR.2016.91.

Ruff, L., Vandermeulen, R., Goernitz, N., Deecke, L., Sidiqui, S. A., Binder, A., Müller, E., and Kloft, M. Deep one-class classification. In *International conference on machine learning*, pp. 4393–4402, 2018.

Schlegl, T., Seeböck, P., Waldstein, S. M., Schmidt-Erfurth, U., and Langs, G. Unsupervised anomaly detection with generative adversarial networks to guide marker discovery. In *International conference on information processing in medical imaging*, pp. 146–157. Springer, 2017.

Senge, R., Bösner, S., Dembczyński, K., Haasenritter, J., Hirsch, O., Donner-Banzhoff, N., and Hüllermeier, E. Reliable classification: Learning classifiers that distinguish aleatoric and epistemic uncertainty. *Information Sciences*, 255:16–29, 2014.

Škvára, V., Pevný, T., and Šmídl, V. Are generative deep models for novelty detection truly better? *arXiv preprint arXiv:1807.05027*, 2018.

Snoek, J., Ovadia, Y., Fertig, E., Lakshminarayanan, B., Nowozin, S., Sculley, D., Dillon, J., Ren, J., and Nado, Z. Can you trust your model’s uncertainty? evaluating predictive uncertainty under dataset shift. In *Advances in Neural Information Processing Systems*, pp. 13969–13980, 2019.

Sünderhauf, N., Brock, O., Scheirer, W., Hadsell, R., Fox, D., Leitner, J., Upcroft, B., Abbeel, P., Burgard, W., Milford, M., et al. The limits and potentials of deep learning for robotics. *The International Journal of Robotics Research*, 37(4-5):405–420, 2018.

Teye, M., Azizpour, H., and Smith, K. Bayesian uncertainty estimation for batch normalized deep networks. In *International Conference on Machine Learning*, pp. 4907–4916, 2018.

van Amersfoort, J., Smith, L., Teh, Y. W., and Gal, Y. Simple and scalable epistemic uncertainty estimation using a single deep deterministic neural network. *arXiv preprint arXiv:2003.02037*, 2020.

Wenzel, F., Roth, K., Veeling, B. S., Świątkowski, J., Tran, L., Mandt, S., Snoek, J., Salimans, T., Jenatton, R., and Nowozin, S. How good is the bayes posterior in deep neural networks really? *arXiv preprint arXiv:2002.02405*, 2020.

Xiao, H., Rasul, K., and Vollgraf, R. Fashion-mnist: a novel image dataset for benchmarking machine learning algorithms. *arXiv preprint arXiv:1708.07747*, 2017.

Zhang, G., Sun, S., Duvenaud, D., and Grosse, R. Noisy natural gradient as variational inference. *arXiv preprint arXiv:1712.02390*, 2017.

A. Appendix

A.1. Background

A.1.1. PROOF OF EQUATION 3.2

Given a deterministic neural network comprised of L layers with $L - 1$ latent representations $(\mathbf{z}_0, \dots, \mathbf{z}_{L-2})$. Since the network is deterministic we know that $p(\mathbf{z}'_i | \mathbf{x}) = \delta(\mathbf{z}'_i - f_i(\mathbf{x}))$ and, consequently, $f_i : x \rightarrow z_i, \forall i$: $p(\hat{\mathbf{y}} | \mathbf{x}) = \int p(\hat{\mathbf{y}} | \mathbf{z}'_i) p(\mathbf{z}'_i | \mathbf{x}) d\mathbf{z}'_i = p(\hat{\mathbf{y}} | \mathbf{z}_i)$ where $\mathbf{z}_i = f_i(\mathbf{x})$. Thus, it follows that $H(\hat{\mathbf{y}} | \mathbf{z}_i) = H(\hat{\mathbf{y}} | \mathbf{x})$. Furthermore, following the data processing inequality, for any deterministic f of a random variable x : $H(x) \geq H(f(x))$. Since the z_i are deterministic functions of the z_{i-1} : $H(\mathbf{x}) \geq H(\mathbf{z}_0) \geq \dots \geq H(\mathbf{z}_{L-2})$.

A.1.2. CONDITIONAL NORMALIZING FLOWS

Normalizing Flows (NFs) (Dinh et al., 2014; 2017) are a family of explicit generative models based on invertible neural networks. Assume we wish to model the distribution p_X of some data X . Given some parametric distribution p_Z and a NF f_θ comprised of weights θ , likelihood evaluation of a data point $x \in X$ in NFs is based on the change of variable formula

$$p_X(x) = p_Z(f_\theta(x)) \left| \det \left(\frac{\partial f_\theta(x)}{\partial x} \right) \right| \quad (5)$$

and made feasible by designing invertible layers that allow evaluating their Jacobian determinant efficiently. One such layer is the coupling layer introduced by (Dinh et al., 2017). Each coupling layer splits its input activations into two sets $u_{1/2}^{in}$ and uses one set u_1^{in} to compute scaling and translation of the other set u_2^{in} using trainable, non-invertible functions g_s and g_t , while it applies the identity function to u_1^{in} .

$$\begin{aligned} u_1^{out} &= u_1^{in} \\ u_2^{out} &= (u_2^{in} + g_t(u_1^{in})) \odot g_s(u_1^{in}) \end{aligned}$$

This transformation renders the Jacobian a lower triangular matrix where the determinant is simply the product of the main diagonal.

Several ways have been proposed to use NFs for modeling the conditional distribution $p_{X|C}$ of $x \in X$ conditioned on some random variable $c \in C$. We adapt the conditioning scheme used in (Ardizzone et al., 2019), where the authors use a conditional version of the above coupling layer. Consequently, the coupling layers in the conditional normalizing flow $f_\theta(x|c)$ become:

$$\begin{aligned} u_1^{out} &= u_1^{in} \\ u_2^{out} &= (u_2^{in} + g_t(u_1^{in}; c)) \odot g_s(u_1^{in}; c) \end{aligned}$$

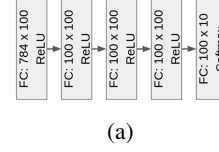


Figure 4: Architecture used in our image classification experiments. Multi-layer perceptron. FC denotes a fully-connected layer.

g_s and g_t are implemented as multi-layer perceptrons. To feed the conditional information into g_s and g_t , we apply a separate multi-layer perceptron to c and add the result to $g_t(u_1^{in})$ and $g_s(u_1^{in})$.

A.2. Image Classification

A.2.1. ARCHITECTURES

The neural networks architectures used in our image classification experiments can be found in fig. 4. We applied the multi-layer perceptron (fig. 4) to MNIST and FashionMNIST and ResNet18 (He et al., 2016b) to CIFAR10 and SVHN.

A.2.2. DEEP ENSEMBLE AND MC DROPOUT

All deep ensembles in section 4.1.1 consist of ten neural networks of the same architecture as used by our approach. When training MC Dropout, we place an additional dropout layer after every dense layer (FCNet) or after every ResBlock (resnet).

A.2.3. TRAINING

We describe the training of the neural networks on image classification and the output-conditional densities on the latent representations separately.

Neural Network Training

We train both, FCNet and resnet, using Adam (Kingma & Ba, 2014) ($\beta_1 = 0.9$, $\beta_2 = 0.999$) and a batch size of 32. We use a learning rate of 0.001 and weight decay of 0.0001. We train the networks for 200 epochs, while performing early stopping with a patience parameter of 20. For all datasets, CIFAR10, SVHN, MNIST and FashionMNIST, we use fixed validation set containing 20% of the training data. All reported results are on the test set of the corresponding dataset.

Output-conditional Density Training

After training the neural networks, we extract the activations of the training data at layers of varying depth with the corresponding prediction of the neural network. Subsequently, we estimate the distribution of the latent representations of

each class prediction with a separate GMM of five components. We use the sklearn GMM implementation⁴. Since the shallow layers of resnet are high-dimensional ($\gg 100$), density estimation - especially in the output-conditional case - becomes challenging. We counter this by reducing the dimensionality of the activations of each layer to 512 using a principal component analysis. Our multi-layer perceptron does not require dimensionality reduction, since each hidden layer has only 100 hidden units.

We also experimented with using NFs for this task. However, we found that a GMM is sufficient to fit the output-conditional distribution of latent representations throughout all layers. The fit of a single multi-variate Gaussian can be qualitatively observed in fig. 5 for FCNet.

A.3. Regression

A.3.1. MODEL TRAINING

For the regression prediction, we train a multilayer perceptron with 50 hidden units and 4 hidden layers until convergence. We then extract latent activations z from the penultimate layer and train a CNF conditioned on the predictions of the multilayer perceptron over the whole training data. Since our training data is relatively small (750 samples), we do not use minibatches in both trainings.

For the ensemble, we take the same perceptron architecture and train 10 models with different random seeds.

The GP has a simple RBF kernel and is fit to the same training data as the perceptron.

A.3.2. EVALUATION

To evaluate eq. 3, we take a range of 1000 support points of $y \in [-10, 10]$ and estimate $p(z|y)$ with the CNF. We further assume a uniform prior $p(y)$ and numerically integrate over the support points to yield $\log p(z)$.

For the visualised confidence regions, we start the integration at the prediction of the regression network and integrate separately in positive and negative direction until the integral reaches the set probability mass. In fig. 3, we visualize the integration boundaries to reach 20% of the probability mass from the CNF.

A.4. Semantic Segmentation

As a large-scale classification experiment, we evaluate our method on semantic segmentation for urban driving. We use the state-of-the-art DeepLabv3+ (Chen et al., 2018) network trained on the Cityscapes urban driving dataset (Cordts et al., 2016a) and estimate the feature density in the last layer

⁴<https://scikit-learn.org/stable/modules/generated/sklearn.mixture.GaussianMixture.html>

method	Misclass. Detection AUROC	OOD Detection	
		AP	FPR ₉₅
softmax entropy	94	2.9	45
mc dropout	-	9.8	38
joint likelihood	70	3.1	24
conditional entropy	92	0.8	100

Table 3: Comparison against softmax entropy and monte-carlo dropout on the two downstream tasks of misclassification and OOD detection. All values in [%].

before the logits.

A.4.1. EXPERIMENTAL SETUP

We use the pre-trained DeepLabv3+ (Chen et al., 2018) provided by the authors⁵ as the base network for the experiments with semantic segmentation. To train the output-conditional GMMs, we extract latent embeddings from the last layer before the logits (decoder_conv1_0) before the relu activation. We found the embedding dimensionality of 256 to be low enough to fit densities directly, without further dimensionality reduction. To associate latent vectors with predicted classes, we interpolate them bilinearly to the output resolution of 1024x2048. To counter the correlations of latent vectors within the same image, we subsample a maximum of 500 vectors for every class and image. We then train the GMMs on a shuffled set of 100000 such vectors. We find suitable hyperparameters for the GMMs on the FishyScapes Lost & Found validation set and use the same hyperparameters for all classes. The best average precision on the validation set was achieved with 2 mixture components per class, tied covariance matrices, 1000 iterations and covariance regularisation factor 0.0001.

For estimating aleatoric uncertainty, we experienced numerical issues when evaluating $p(\hat{y}|\mathbf{z}^*)$. This is due to the normalization $\sum_y p(\hat{y}|\mathbf{z}^*) = 1$ when some classes are much more likely than others, i.e. when the entropy is low. We counteract these numerical issues by evaluating $h(\hat{y}|\mathbf{z}^*)$ on underfit GMMs⁶ and on embedding vectors that were interpolated to output resolution (which was not found necessary for epistemic uncertainty and significantly increases memory usage). We show qualitative examples of the estimated uncertainties in figure 7.

⁵https://github.com/tensorflow/models/blob/master/research/deeplab/g3doc/model_zoo.md#deeplab-models-trained-on-cityscapes

⁶1 component, only 50 iterations, covariance regularisation with 0.1

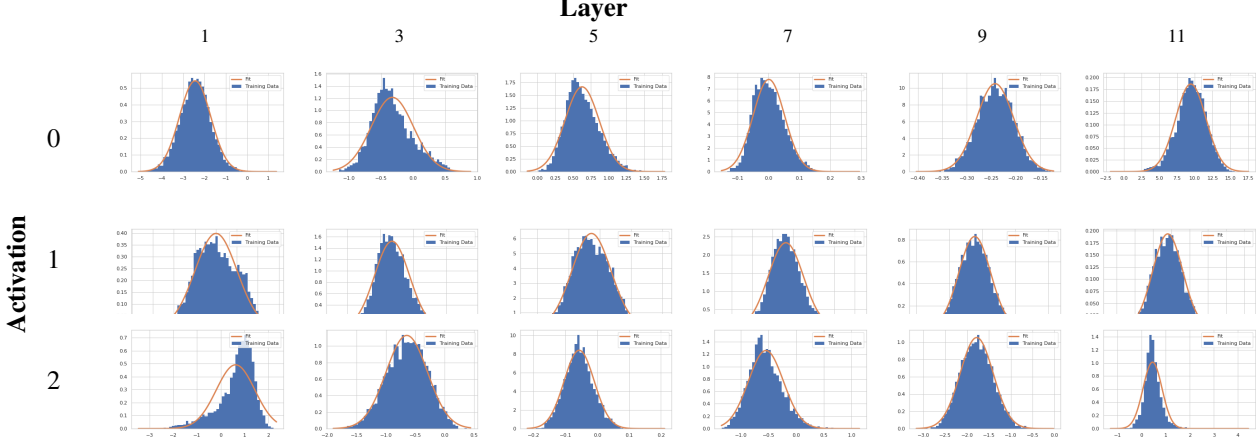


Figure 5: Empirical output-conditional (class 0) distribution of latent representations (blue) of the multi-layer perceptron obtained from the training data (MNIST). Columns represent the different layers used in our experiments (layer 1, 3, 5, 7, 9, 11) and each row shows a different neuron. We also plot the corresponding multivariate Gaussian projected onto the respective dimension. We observe that the output-conditional activations are approximately Gaussian distributed.

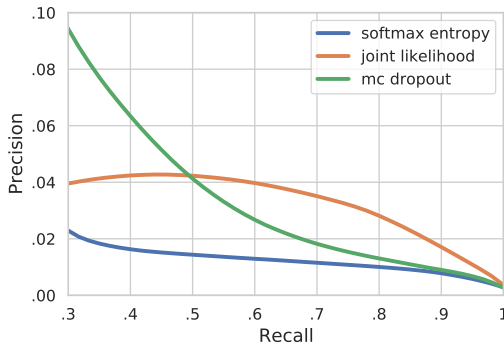


Figure 6: Precision-Recall curve for OOD detection on the FishyScapes benchmark. The shown high-recall region is especially important for safety-critical applications.

A.4.2. RESULTS

We test the estimation of aleatoric uncertainty by measuring the performance for misclassification detection on the Cityscapes validation data. Due to the nature of misclassifications, which are caused by the network itself, we can only directly compare against other methods that work on the exact same network. For OOD detection, we evaluate on the FishyScapes anomaly detection benchmark (Blum et al., 2019) and report the results in table 3 and figure 6. We find that our method performs especially well in the safety-critical high recall discipline, where it outperforms all other unsupervised methods (i.e. not trained on OOD data) in the FPR₉₅ metric (false positive rate at 95% true positive rate).

Overall, we find that the joint estimation of aleatoric and

epistemic uncertainty scales without problems to this complex task. As expected, density estimation is a good method for OOD detection.

A.5. Depth Regression

We apply our framework to the large-scale task of monocular depth regression on KITTI (Geiger et al., 2012).

A.5.1. EXPERIMENTAL SETUP

We use a pretrained model from (Godard et al., 2017)⁷ trained on KITTI and extract the activations z from the penultimate layer (output of the penultimate convolution) on the training data and the corresponding depth prediction. We need to estimate two densities: the output-conditional density $p(\mathbf{z}^*|\hat{\mathbf{y}})$ and the density of the predictions $p(\hat{\mathbf{y}})$.

Output-conditional Density of Latent Representations

The conditional density $p(\mathbf{z}^*|\hat{\mathbf{y}})$ is shared across all pixels. To assemble a dataset for training the density model on the training data, we extract the depth predictions pixel-wise and all activations that are in the corresponding receptive field. This leads to a 144 dimensional distribution conditioned on a scalar depth prediction. We randomly extract 12800 samples from the 256×512 dimensional depth maps and shuffle the resulting dataset to ensure that correlations between adjacent pixels have a minimal impact on the i.i.d. assumption when training the CNF. Subsequently, we train a conditional version of the RealNVP (Dinh et al., 2017) on the resulting dataset, where we use a conditioning scheme similar to the one used by (Ardizzone et al., 2019) (see

⁷<https://github.com/mrhariicot/monodepth>

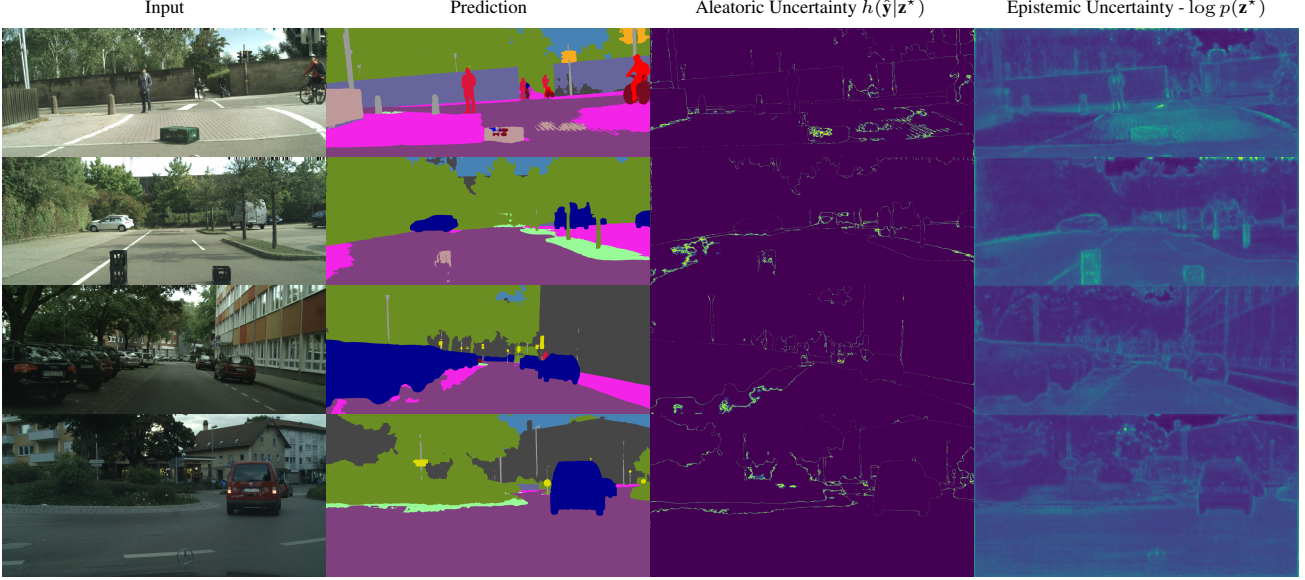


Figure 7: Qualitative examples of the estimated uncertainties for semantic segmentation. Rows 1 and 2 are examples from the Lost & Found dataset with OOD objects (Pinggera et al., 2016), rows 3 and 4 from the Cityscapes validation set (Cordts et al., 2016b). As expected, aleatoric uncertainty increases around object boundaries and is higher for uncertain classifications, whereas epistemic uncertainty is low on the validation set and high for anomalous objects and the uncommon street texture in the first row.

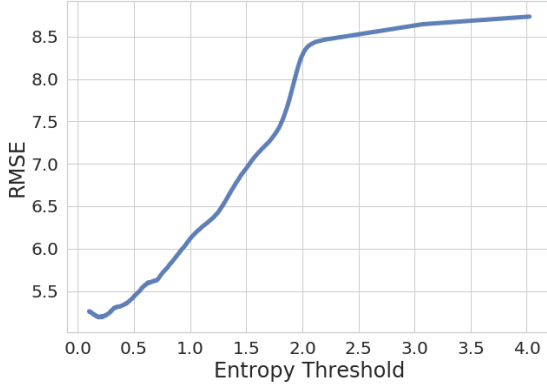


Figure 8: Average RMSE for a monocular depth prediction network (Godard et al., 2017) trained on KITTI (Geiger et al., 2012), accumulated below the given threshold of aleatoric uncertainty $h(\hat{y}|z^*)$. As expected of aleatoric uncertainty, it increases monotonically for larger errors.

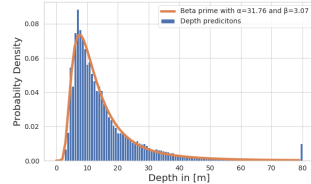


Figure 9: Fitting distribution of depth predictions with univariate beta prime distribution. We visualize normalized histogram of predicted depth values using a pretrained model from (Godard et al., 2017) and a beta prime distribution with parameters $\alpha = 31.76$ and $\beta = 3.07$. The small peak of the predicted depth values at 80m is an artifact of the code on which we base this experiment, since they clip depth predictions at 80m.

section A.1.2). Our RealNVP consists of 3 coupling layers where scaling and translation are each computed using a separate multi-layer perceptron with 2 hidden layers of each 100 dimensions. We refer to the original work (Dinh et al., 2017) for a general description of the RealNVP. We train the CNF using Adam optimizer with learning rate $1e - 6$ and weight decay $1e - 5$. We further use a batch size of 128 and use early stopping with a patience parameter of 20.

Parametric Distribution of Depth Predictions

We empirically found that the distribution of depth predictions on the training data is well represented by a univariate

beta prime distribution with $\alpha = 31.76$ and $\beta = 3.07$.

Fig. 9 shows the quality of this estimate.

Evaluation of Aleatoric Uncertainty

Evaluating aleatoric uncertainty requires computing $h(\hat{\mathbf{y}}|\mathbf{z}^*) = - \int d\hat{\mathbf{y}} p(\hat{\mathbf{y}}|\mathbf{z}^*) \log(p(\hat{\mathbf{y}}|\mathbf{z}^*))$ where $p(\hat{\mathbf{y}}|\mathbf{z}^*) = \frac{p(\mathbf{z}^*|\hat{\mathbf{y}})p(\hat{\mathbf{y}})}{p(\mathbf{z}^*)}$ and $p(\mathbf{z}^*)$ is obtained by marginalizing over $\hat{\mathbf{y}}$.

Since the depth predictions in our experiment are only one-dimensional, computing $h(\hat{\mathbf{y}}|\mathbf{z}^*)$ is achieved in a straightforward manner using numerical integration. We discretize the interval of observed depth values [3, 80] with 154 supporting points with equidistant spacing of 0.5. Note that for higher-dimensional $\hat{\mathbf{y}}$ above integral can be solved more efficiently using importance sampling.

A.5.2. RESULTS

We evaluate the quality of the aleatoric uncertainty. We compute $h(\hat{\mathbf{y}}|\mathbf{z}^*)$ according to eq. equation 4 and evaluate its correlation with the RMSE in fig. 8. As expected, larger errors have larger aleatoric uncertainty. We conclude that the aleatoric uncertainty estimate scales to large regression networks.